International Journal of Applied Earth Observations and Geoinformation 109 (2022) 102772

Contents lists available at ScienceDirect

International Journal of Applied Earth Observations and Geoinformation

journal homepage: www.elsevier.com/locate/jag

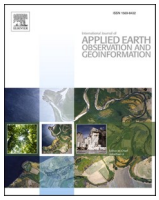

# Improving UAV-SfM time-series accuracy by co-alignment and contributions of ground control or RTK positioning

E.W. Nota, W. Nijland, T. de Haas *

*Department of Physical Geography, Utrecht University, Utrecht 3584 CB, the Netherlands*

ARTICLE INFO

*Keywords:*
UAV
SfM photogrammetry
Co-alignment
Time-SIFT
Ground Control Points
Change detection

ABSTRACT

Unmanned Aerial Vehicle Structure from Motion (UAV-SfM) photogrammetry is increasingly applied to topographic change detection, which requires multitemporal Digital Surface Models (DSMs) with high relative accuracy. Of these tools, Ground Control Points (GCPs) and an image processing method called co-alignment have so far shown promising results for change detection studies. However, there is still insufficient research on the extent of improving 3D model accuracy by combining these tools. In our study we assess absolute and relative accuracy of 120 DSMs generated through 24 workflows of UAV-SfM photogrammetry. Surveys were acquired with two different UAVs with Real Time Kinematic (RTK) or generic Global Navigation Satellite System (GNSS) positioning, and processed with varying combinations of survey co-alignment and GCPs. We show that co-alignment reduces relative errors to below 2 cm regardless of positioning quality. A single RTK survey in a co-aligned project is sufficient to obtain high absolute xy accuracy, but GCPs for at least one survey are still required to reduce absolute z error. We demonstrate that co-aligning RTK surveys with generic GNSS surveys results in RTK class accuracy for all surveys, even when mixed sensor grades are used. Our findings enable high-accuracy change detection with lower accuracy archived images when combined with RTK surveys. For future UAV-SfM change detection studies, we recommend to apply co-alignment for all studies, and where possible to include GCPs and RTK image coordinates in one survey to optimize absolute accuracy. Collecting and digitizing GCPs in multiple surveys has shown little additional benefit when co-alignment is applied and therefore may be omitted to save time, especially in challenging field conditions.

## 1. Introduction

Since the beginning of the century, the application of Unmanned Aerial Vehicles (UAVs) has expanded from military to civilian use, encouraged by rapid developments of UAV design, flight control and sensor accuracy (Nebiker et al., 2008; Fonstad et al., 2013), as well as increased accuracy of Global Navigation Satellite Systems (GNSS) and Inertial Measurement Units (IMUs) (Turner et al., 2012). Amongst these emerging UAV applications is topographic mapping using 'Structure from Motion' (SfM) photogrammetry (e.g. Turner et al., 2012; Westoby et al., 2012; James et al., 2017; Anderson et al., 2019). SfM techniques principally refer to the computation of 3-D structures by automatically simultaneously estimating camera and point geometry of a series of overlapping images (Snavely, 2008; Westoby et al., 2012). In recent years, SfM photogrammetry has undergone a fruitful development because of technical improvements, enhanced methodologies, software improvement, and increased access due to low-budget equipment (Anderson et al., 2019).

Anderson et al. (2019) describe a wide range of UAV-SfM topographic mapping applications. Of special interest for this study is change detection of a topographic surface. At a given location, topographic change between two different time steps can be mapped by subtracting UAV-SfM derived Digital Surface Models (DSMs) of these time steps, creating a so-called DSM of Difference (DoD) map. However, DSM inaccuracy due to model and measurement uncertainties in terms of absolute representation of the field, relative location between both DSMs, and spatial variability presents a significant challenge in DoD applications (Wheaton et al., 2009; Bakker & Lane, 2017; James et al., 2017; Zhang et al., 2019; De Haas et al., 2021). An often occurring feature of spatial error is a doming surface, where the DSM boundaries show higher offsets than the centre (Przybilla et al., 2020). Moreover, DSM accuracy can depend significantly on surface roughness, as photogrammetry methods have a smoothening effect on objects and rough surfaces (Smith et al., 2004; Jester & Klik, 2005; Cook, 2017). It is

* Corresponding author.
*E-mail address:* T.deHaas@uu.nl (T. de Haas).

https://doi.org/10.1016/j.jag.2022.102772
Received 5 November 2021; Received in revised form 24 March 2022; Accepted 3 April 2022
Available online 28 April 2022

therefore evident that high resolution images are essential to create accurate DSMs for change detection research (Bakker & Lane, 2017).

Two main methods exist for georeferencing SfM projects: Direct Georeferencing (DG), and indirect referencing using Ground Control Points (GCPs). Direct Georeferencing constructs DSMs using the directly measured position and orientation of the UAV camera, where position is defined by three coordinates (x, y, z) and orientation by three rotation angles (usually roll, pitch, yaw) (Pfeifer et al., 2012). However, the reliability of the measurements is strongly dependent on sensor quality, which is usually low for low-cost devices due to weight and cost restrictions (Gerke & Przybilla, 2016). Yet, great improvements in UAV-SfM derived model accuracies have been made through increased availability of Real Time Kinematic (RTK) positioning systems on-board UAVs (Stempfhuber & Buchholz, 2011; Gerke & Przybilla, 2016). RTK systems determine positions by real-time processing GNSS signals measured on the UAV platform with signals from a stationary base station resulting in positioning accuracy at cm-level (Takasu & Yasuda, 2009). Indirect georeferencing based on GCPs is more time-consuming and labour intensive, requiring distributed field measurements throughout the fieldwork area as well as extensively digitizing GCPs in the collected UAV images (Aicardi et al., 2016; Li et al., 2017; Saponaro et al., 2021). Moreover, indirect georeferencing is impractical or even impossible when studying hazardous or inaccessible environments or, in the case of change detection, GCPs can get moved or lost over time (De Haas et al., 2020). Finally, areas without GCPs may still result in locally highly inaccurate DSMs (Li et al., 2017). Besides practical considerations, indirect georeferencing is less accurate than direct georeferencing when based on similar point positioning precision due to more degrees of freedom in the bundle adjustment and usually fewer available control positions. In addition, change detection errors between surveys are cumulative (James et al., 2017), resulting in unreliable DoDs.

Aside from developments in on-board positioning systems, an image processing technique, referred to as co-alignment (e.g. Cook & Dietze, 2019), United Bundle Adjustment (UBA) (Li et al., 2017), time-SIFT (e.g. Feurer & Vinatier, 2018) or Multi-Epoch and Multi-Imagery (MEMI) (Blanch et al., 2021), has proven promising for improving UAV-SfM constructed models. The conventional UAV-SfM approach creates 3D models from each survey individually, while co-alignment creates multi-temporal models by processing UAV imagery from multiple surveys as a single block during the alignment step (Feurer & Vinatier, 2018). Prior to the initial development of co-alignment, Aicardi et al. (2016) applied an automated co-registration technique where a reference survey is used to define fixed orientation parameters, to which the geometries of other surveys are aligned. As Li et al. (2017) point out, this co-registration is still prone to large errors due to local inaccuracies of the reference survey alignment. To counter this, co-alignment omits the step of defining a reference geometry and processes all desired UAV surveys simultaneously into a unified coordinate system with relative accuracy (Li et al., 2017). So far, co-alignment of UAV-SfM topographic mapping applications has been explored in several studies. Li et al. (2017) showed a higher accuracy for change detection in an urban development study when co-alignment is applied. Feurer & Vinatier (2018) showed that co-alignment results in consistent DSMs for different time steps when using GCPs of low accuracy. Cook and Dietze (2019) used co-alignment to construct topographic change without using GCPs, resulting in significantly reduced relative errors between the DSMs as compared to using the classical approach with GCPs. Hendrickx et al. (2020) showed the possibility of co-alignment with different UAV sensors with RTK settings, while Parente et al. (2021) found that co-alignment worked well when using both UAV as well as terrestrial imagery at varying spatial and temporal scales as well as weather and illumination conditions without RTK settings. De Haas et al. (2021) found a great improvement in relative accuracy and minor improvement of absolute accuracy when using co-alignment with GCPs compared to the classical approach. They moreover showed a significant improvement for relative errors when applying co-alignment without GCPs, showing the potential of co-alignment for topographic change detection as it greatly improves the relative positioning of DSMs that are poorly aligned when processed individually. Blanch et al. (2021) explored the possibility of fully automating the co-alignment workflow from capturing images to creating DoDs and found improvements of overall errors in the order of 1.1 to 3.0 cm without using GCPs. Finally, Saponaro et al. (2021) showed that co-alignment is also a robust method for comparing point clouds in change detection studies.

Several studies have so far applied co-alignment with SfM for UAV (Dietze et al., 2020; Fojtik, 2020; Hendrickx et al., 2020; Dille et al., 2021) as well as satellite imagery (Watson et al., 2020), underlining the effectiveness of the workflow. However, the full potential of co-alignment has not been completely studied, leaving questions with respect to the extent of reliability, applicability, and efficiency of co-alignment. A potential application is in UAV monitoring programmes with archived data collected with low positioning accuracy where RTK surveys are included at a later stage. It remains uncertain if existing surveys can be improved to the accuracy of RTK surveys by using co-alignment.

The main objective of our study is to quantify the accuracy of UAV-SfM generated DSMs using co-alignment, GCPs, RTK surveys and generic GNSS surveys. A total of 24 scenarios were defined for multiple UAV surveys in idealized field conditions on an artificial hill in The Netherlands to study the absolute and relative errors of the created DSMs. The scenarios were designed to study the effects of co-alignment of surveys with mixed positioning precision (e.g. only few surveys have RTK or GCPs, or some surveys use lower grade sensors) in order to answer the following research questions:

- What are the differences between the accuracies of conventional GNSS and RTK surveys when applying either direct georeferencing, indirect georeferencing, co-alignment or a combination of both co-alignment and indirect georeferencing?
- To what extent do GCPs improve accuracy when using co-alignment with RTK surveys? Is ground control needed in all surveys or is digitizing GCPs in one survey sufficient?
- What is the effect of co-aligning surveys of an RTK platform with surveys obtained using a consumer grade UAV?

The co-aligned scenarios are compared to individually processed surveys with RTK and conventional GNSS accuracies processed with either direct georeferencing or GCPs. For each scenario, 5 separate surveys are processed to obtain a reliable estimate of the relative differences between the obtained DSMs. Absolute accuracies are determined against the positions of 21 validation targets placed on the ground. In our study, we present a straightforward comparison between the 24 scenarios of these relative and absolute errors. We aim to contribute to the ongoing development of UAV-SfM image processing research, and in particular for change detection studies.

## 2. Methods

### 2.1. Study site

UAV surveys were conducted over the Nedereindse Berg (52.04°N, 5.06°E) in the province of Utrecht, The Netherlands (Fig. 1). The Nedereindse Berg is an artificial mound used for recreational purposes, has an elevation between 1.0 and 16.0 m a.s.l. and an area of 0.12 $km^2$. It hosts road cycling and skating tracks, and is predominantly covered by grass and some trees.

### 2.2. Data acquisition

Images of the Nedereindse Berg were captured through 15 surveys during a four-day period, between 1 February 2021 and 4 February 2021. Because the aim of the study is to investigate the full potential of

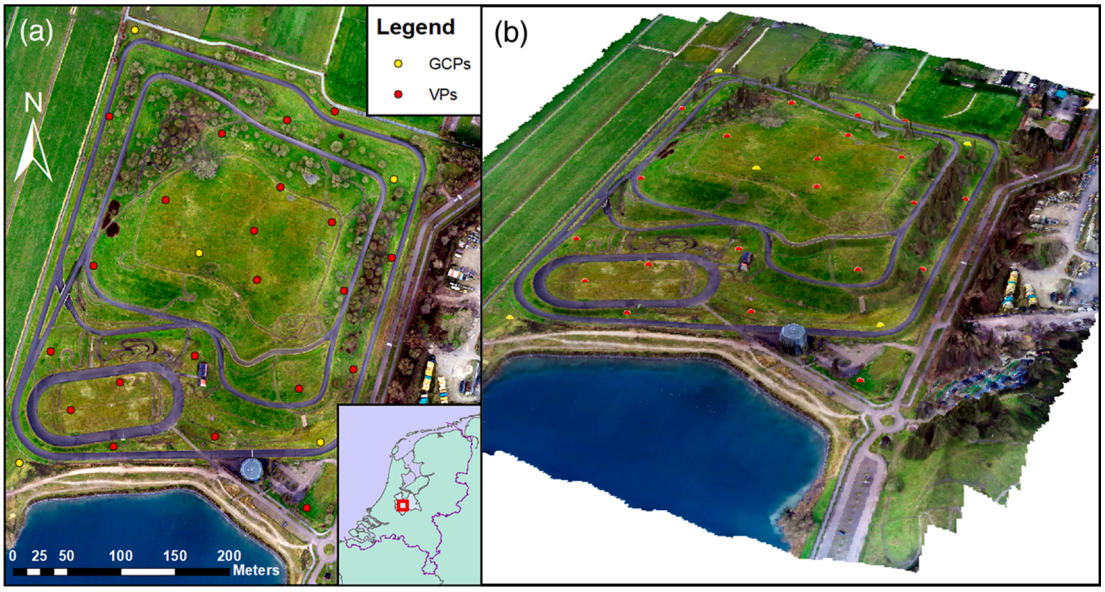


**Fig. 1.** Study area of the Nedereindse Berg. (a) Orthophoto with the locations of GCPs and VPs. (b) 3D view of the area with a vertical exaggeration of 2. Imagery is from RTK survey 1 and was generated under the settings of scenario 8 (full RTK & GCPs, no co-alignment).

applying combinations of GCPs with co-alignment of surveys with multiple sensor settings, the circumstances were deliberately chosen to be idealized. During the survey period, no changes occurred on the surface, such that each recorded deviation between surveys can be attributed to the inaccuracies of the processing methods. The only difference between the surveys were the lighting conditions, as the surveys varied in times of day and between sunny and partially clouded.

Surveys were flown with a DJI Phantom 4 RTK (20 Mpix, 1″ CMOS sensor. 84° FOV) and DJI Mavic 2 Pro (20Mpix, 1″ CMOS sensor, 77° FOV) (SZ DJI Technology Co., Ltd., 2020). The Phantom 4 is optimized for mapping and has high precision RTK positioning on-board with nominal RMS accuracy of 1 cm + 1 ppm horizontal and 1.5 cm + 1 ppm vertical. The Mavic 2 pro is a high end consumer grade UAV with a generic GNSS system (GPS + GLONASS) with point precision in the order of metres. We use the term 'generic GNSS' to refer to standard grade GNSS methods that use Single Point Processing and do not apply Carrier Phase Enhancement. The Phantom 4 RTK gives similar accuracy when the RTK mode is not used and or no connection to a base station or network RTK provider is available during operation.

Three types of surveys were conducted: (i) Phantom 4 RTK with RTK enabled; (ii) Phantom 4 RTK with generic GNSS positioning (RTK disabled); (iii) DJI Mavic 2 Pro with generic GNSS positioning. All three survey types were flown directly after each other on five different occasions, therefore being numbered between 1 and 5. All flights were conducted along a pre-set flight path with an image overlap of 80% in along and between path directions at an elevation of 100 m above ground level. Images were taken with default settings, at base ISO, with fast shutter-speed priority to avoid motion blur, and stored in jpeg format.

Prior to the UAV surveys, 26 targets of 0.5 by 0.5 m with a checkerboard pattern were evenly distributed over the survey area, similar to the methodology of previous studies (e.g. Fazeli et al., 2016; Gabrlik et al., 2018). Of these targets, 5 were used as GCPs and 21 as validation points (VPs) (Fig. 1). Each Phantom 4 survey captured 340 images, while each Mavic 2 survey captured 260 images, resulting in 1.3 and 1.9 GCPs per 100 images for each sensor, respectively, which is well above the recommended minimum of 1 GCP per 100 images for creating reliable DSMs (Sanz-Ablanedo et al., 2018). Moreover, the GCPs were evenly distributed, as several studies have shown that this results in the most reliable DSMs (Sanz-Ablanedo et al., 2018; Villanueva & Blanco, 2019; Cabo et al., 2021). To assure minimum change of target elevation due to compaction of underlying grass, each target was tightly strung over a wooden block below its centre. Using a Trimble R8 series network RTK GNSS system, the x- and y-coordinates as well as the elevation were measured before the first and after the last UAV survey. The deviation between the surveys was ~ 1–2 cm, falling well within the accuracy of the Trimble R8 system of 2 cm, which we define as the theoretical maximum relative and absolute accuracy.

### 2.3. Data processing

The data were processed with Agisoft Metashape Pro (v. 1.7.1). Photo alignment was performed at high-quality default settings with a key point limit of 40,000 and a tie point limit of 5,000. In the relevant scenarios, GCPs were included to all images they appear on for the surveys of interest. Positioning error estimates for the images were taken from the exif data for the RTK flights and were in the order of 1–3 cm, while for generic GNSS the error was set to a default of 10 m. Camera models were seeded only with available base parameters (image size and focal length) and calibrated as part of the bundle adjustment; alignment and camera parameters were optimized in steps after removing (i) tie points present in less than three images, (ii) with a reconstruction uncertainty larger than 20, (iii) with a projection accuracy larger than 8, and (iv) a reprojection error larger than 0.5. Alignment was run at a HPC cluster with for each node two AMD EPYC 7451 24-Core Processors, 256 GiB memory, and a GeForce GTX 1080Ti graphics card; each scenario aligned within 2 h on a single node. Dense clouds were generated at high quality and mild depth filtering, after which all points with a confidence $< 4$ were removed. DSMs were generated from the dense cloud at high quality settings, and exported with a ground sampling distance of 5 cm. Orthophotos were generated from the DSM with a mosaic blending mode, and exported with a ground sampling distance of 2.5 cm.

### 2.4. Scenarios

Based on the research questions, we defined 24 scenarios, which were grouped in 6 clusters based on the amount of RTK surveys used for processing (Table 1; Fig. 2). Within these clusters, scenarios differed from one another in terms of: (i) whether co-alignment was used, where scenarios 1, 2, 7 and 8 provide the general approach of individually processing surveys to be compared to the other scenarios were co-alignment was applied, (ii) whether GCPs were used and, for the co-alignment scenarios, (iii) for how many surveys the GCPs were digitized. Any of these scenarios either

processes the surveys individually through direct or indirect georeferencing, uses the co-alignment approach or combines co-alignment with digitizing GCPs for at least one survey.

For each scenario, 5 UAV surveys were used, resulting in the computation of 5 DSMs per scenario and thus 120 DSMs in total. In order to be consistent for all scenarios, all survey numbers 1 to 5 were used for data processing (e.g. the Phantom 4 RTK with RTK enabled surveys 1 to 5 were used for the full RTK scenarios 7 to 12). For the scenarios with one RTK survey, RTK survey 5 was used, whereas RTK surveys 4 and 5 were used for the scenarios with two RTK surveys (Table 1).

For convenience, Table 1 also includes ID's for each scenario, which summarize the specific workflow characteristics of the respective scenario, where: (i) 'RTK(x)' refers to the × amount of RTK surveys used; (ii) if relevant, 'P' or 'M' indicate the sensor (Phantom 4 RTK or Mavic 2 Pro) used for the non-RTK surveys; (iii) 'GCP(x)' refers to the × amount of surveys where GCPs were digitized; and (iv) 'Ind' illustrates that the surveys were processed individually, whereas 'CA' indicates that co-alignment was applied. These ID's are further used in this study to

**Table 1**
Scenarios for generating the DSMs in this study.

| Cluster | Scenario | Nr. RTK surveys | Nr. No-RTK surveys | Co-alignment | GCPs | Nr. Surveys with GCPs | No-RTK surveys sensor | Scenario ID |
|---|---|---|---|---|---|---|---|---|
| No-RTK scenarios | 1 | 0 | 5 | No | No | 0 | Phantom | RTK0-P-GCP0-Ind |
| | 2 | 0 | 5 | No | Yes | 5 | Phantom | RTK0-P-GCP5-Ind |
| | 3 | 0 | 5 | Yes | No | 0 | Phantom | RTK0-P-GCP0-CA |
| | 4 | 0 | 5 | Yes | Yes | 5 | Phantom | RTK0-P-GCP5-CA |
| | 5 | 0 | 5 | Yes | Yes | 1 | Phantom | RTK0-P-GCP1-CA |
| | 6 | 0 | 5 | Yes | Yes | 2 | Phantom | RTK0-P-GCP2-CA |
| Full RTK scenarios | 7 | 5 | 0 | No | No | 0 | | RTK5-GCP0-Ind |
| | 8 | 5 | 0 | No | Yes | 5 | | RTK5-GCP5-Ind |
| | 9 | 5 | 0 | Yes | No | 0 | | RTK5-GCP0-CA |
| | 10 | 5 | 0 | Yes | Yes | 5 | | RTK5-GCP5-CA |
| | 11 | 5 | 0 | Yes | Yes | 1 | | RTK5-GCP1-CA |
| | 12 | 5 | 0 | Yes | Yes | 2 | | RTK5-GCP2-CA |
| 1 RTK scenarios | 13 | 1 | 4 | Yes | No | 0 | Phantom | RTK1-P-GCP0-CA |
| | 14 | 1 | 4 | Yes | Yes | 5 | Phantom | RTK1-P-GCP5-CA |
| | 15 | 1 | 4 | Yes | Yes | 1 | Phantom | RTK1-P-GCP1-CA |
| | 16 | 1 | 4 | Yes | Yes | 2 | Phantom | RTK1-P-GCP2-CA |
| 2 RTK scenarios | 17 | 2 | 3 | Yes | No | 0 | Phantom | RTK2-P-GCP0-CA |
| | 18 | 2 | 3 | Yes | Yes | 5 | Phantom | RTK2-P-GCP5-CA |
| | 19 | 2 | 3 | Yes | Yes | 1 | Phantom | RTK2-P-GCP1-CA |
| | 20 | 2 | 3 | Yes | Yes | 2 | Phantom | RTK2-P-GCP2-CA |
| No-RTK MAVIC scenarios | 21 | 2 | 3 | Yes | No | 0 | MAVIC | RTK2-M-GCP0-CA |
| | 22 | 2 | 3 | Yes | Yes | 5 | MAVIC | RTK2-M-GCP5-CA |
| | 23 | 1 | 4 | Yes | No | 0 | MAVIC | RTK1-M-GCP0-CA |
| | 24 | 1 | 4 | Yes | Yes | 5 | MAVIC | RTK1-M-GCP5-CA |

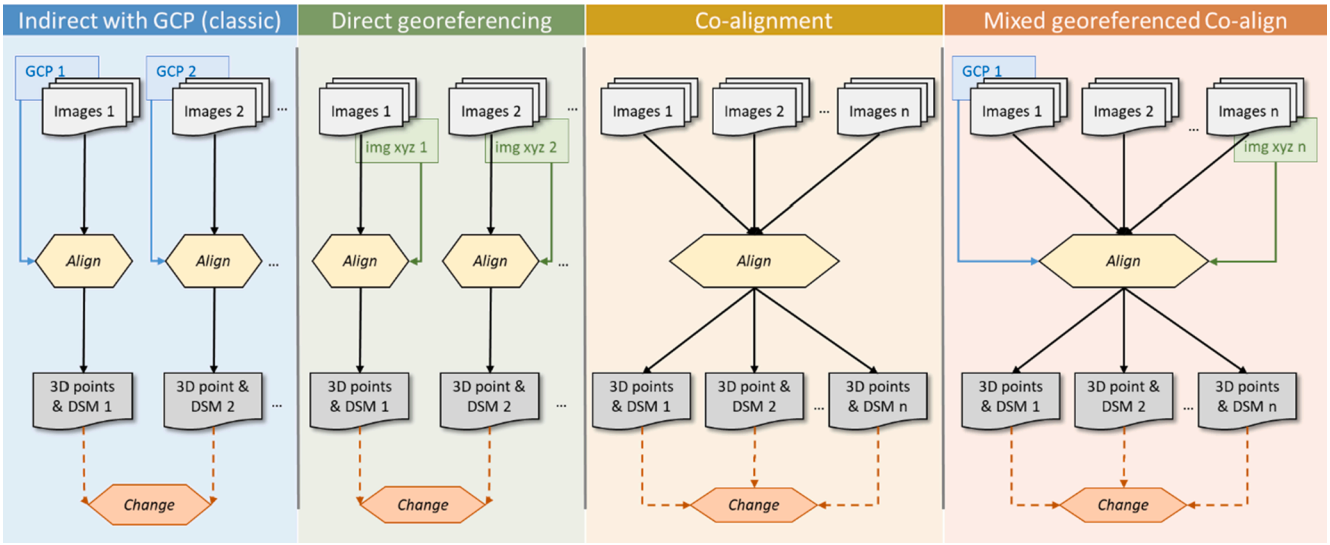


**Fig. 2.** Generic workflows of the methods used in this study, displaying indirect georeferencing with GCPs, direct georeferencing, co-alignment and a mixed workflow. In the diagram the numbers 1,2,.n refer to different collections or acquisition moments indicating the sets of images and corresponding ground control (GCP), high accuracy image coordinates (img xyz), and corresponding resulting products after processing (3D points and DSM).

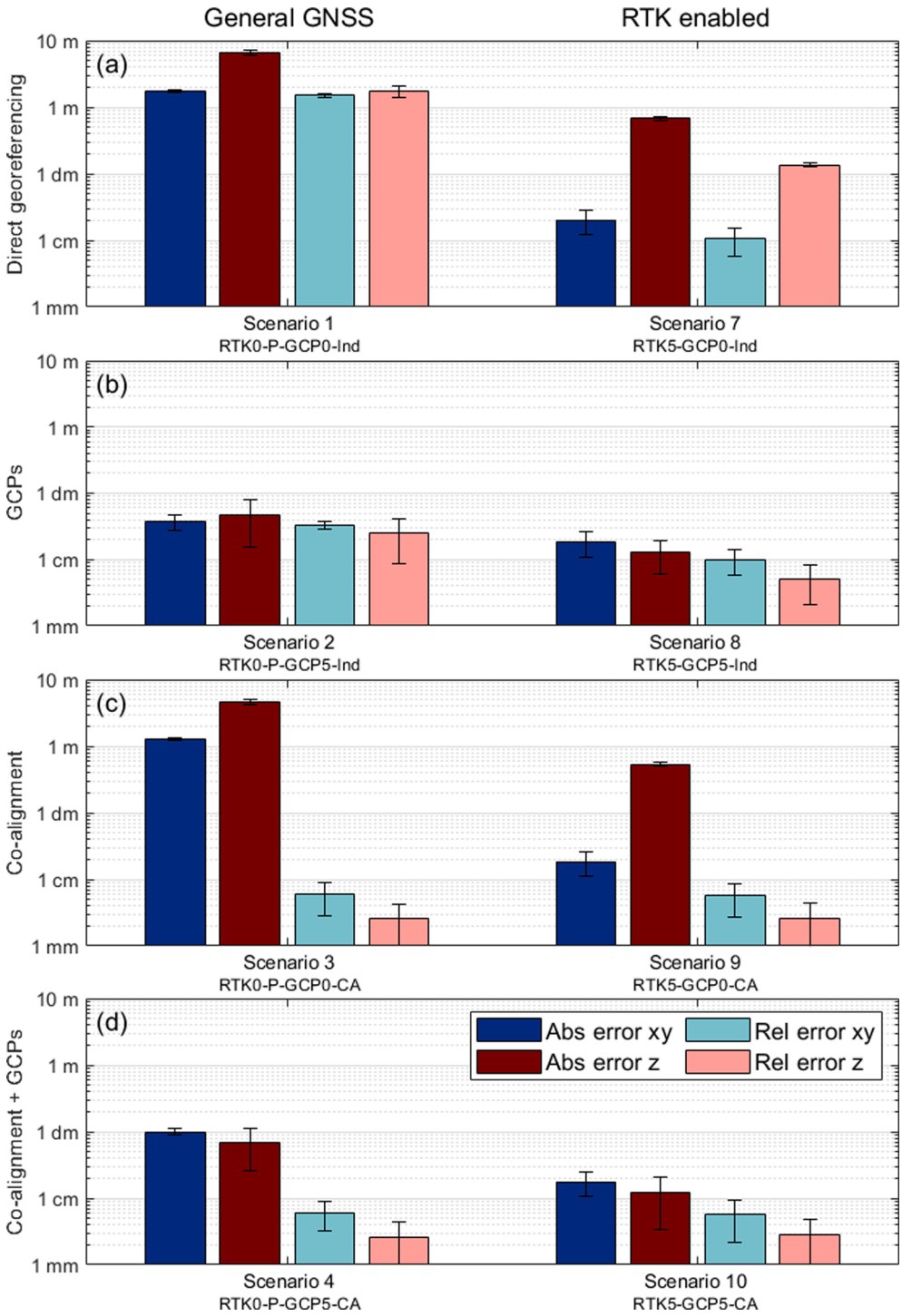


**Fig. 3.** Mean xy and z absolute and relative errors on logarithmic scales for both general GNSS (left) and RTK (right) workflows, with: (a) direct georeferencing; (b) indirect georeferencing with GCPs; (c) co-alignment; (d) co-alignment combined with GCPs. The scenario numbers and respective ID's below each set refer to Table 1. Whiskers on the bars indicate standard deviations.

allow for the direct understanding of the workflow of each scenario.

### 2.5. Data analysis

For all 120 DSMs, we determined both absolute and relative accuracy. The absolute accuracy was quantified by manually extracting the co-ordinates and elevation of all GCPs and VPs of the centre of each target in ArcGIS Pro and calculating the offset from the x, y and z measurements in the field by the Trimble R8 system network RTK GNSS system. As the data showed insignificant differences between x and y errors, the Euclidian distance of xy was used. The DSM with the lowest average absolute z error was used to create DoDs with all the other DSMs to study spatial patterns in accuracy, such as doming (Przybilla et al., 2020).

Relative accuracy was determined by computing the average xy and z values of all 5 surveys for each of the 24 scenarios. The offset from these scenario-specific averages from the planimetric xy and altimetric z values of each DSM within the same scenario, were considered the relative errors.

Aside from comparing the absolute and relative errors, *t*-tests ($\alpha =$

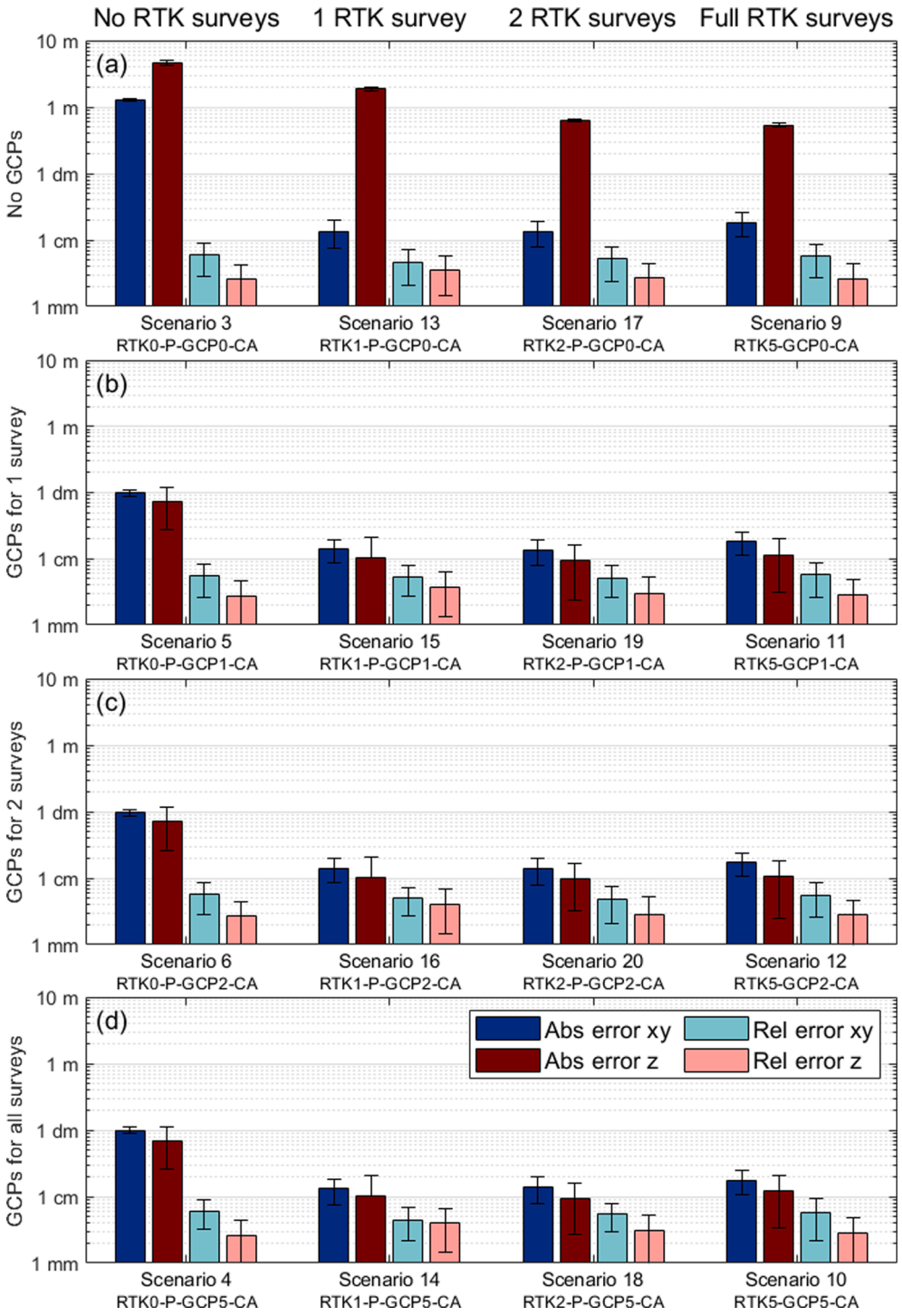


**Fig. 4.** Mean xy and z absolute and relative errors on logarithmic scales for the co-alignment scenarios where we varied the number of RTK surveys used and the number of surveys for which all GCPs were digitized. (a) GCPs were not digitized; (b) GCPs were digitized for 1 survey; (c) GCPs were digitized for 2 surveys; and (d) GCPs were digitized for all surveys. The scenario numbers and respective ID's below each set refer to Table 1. Whiskers on the bars indicate standard deviations.

0.05) were performed for the absolute xy and z errors to test whether the errors show equal means between the surveys within each scenario as well as each survey between all scenarios. For the latter, only the same surveys (e.g. Survey 1) between all scenarios were compared, as these general GNSS Phantom 4, RTK Phantom 4, and general GNSS Mavic 2 Pro surveys were all flown immediately after each other, assuring as little change in the field and weather conditions as possible.

## 3. Results

The following section systematically describes the results structured per research question mentioned in section 1. First, we compare the results of the scenarios with all surveys conducted through generic GNSS with those through RTK. Then we explore the effects of varying the amount of surveys for which GCPs are digitized, after which we provide the effects of co-alignment and GCPs of using both the Phantom 4 and Mavic 2 Pro UAV. Lastly, we show more detailed results of the differences between surveys

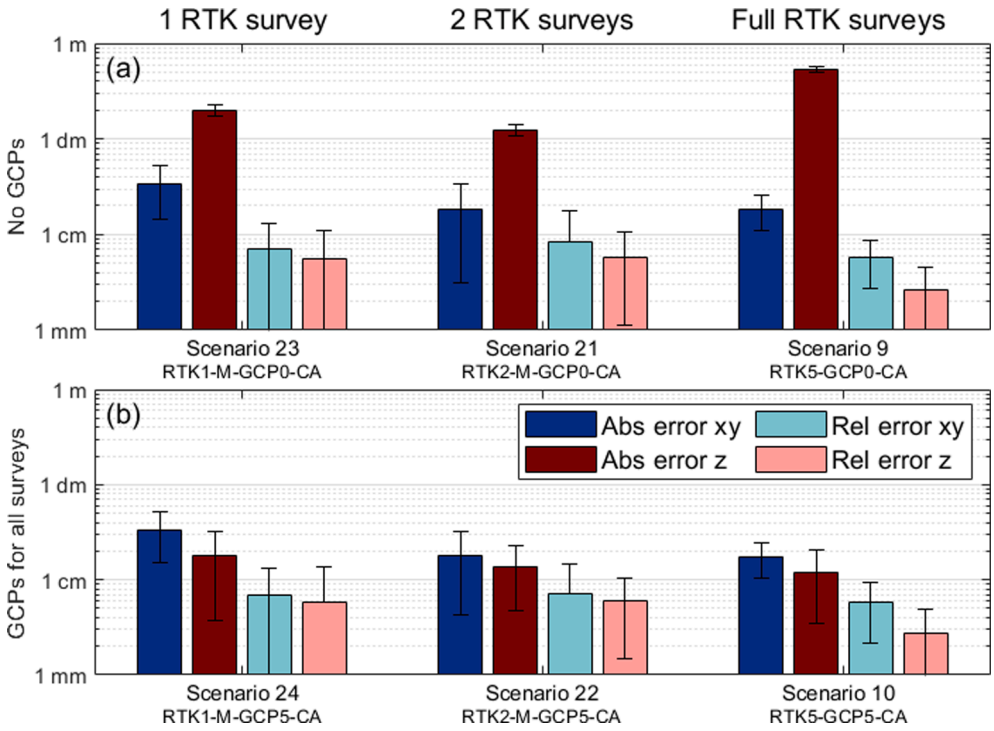


**Fig. 5.** Mean xy and z absolute and relative errors where DJI Phantom 4 RTK surveys are co-aligned with DJI Mavic 2 Pro surveys with generic GNSS as well as co-alignment of all DJI Phantom RTK surveys, where (a) GCPs are not digitized in any of the surveys and (b) GCPs are digitized for all surveys. The scenario numbers and respective ID's below each set refer to Table 1. Whiskers on the bars indicate standard deviations.

within some generic scenarios. The average results of the absolute and relative errors as well as their standard deviation in both xy and z directions, are provided in Table A1 in the appendix.

### 3.1. Co-alignment in homogeneous sets: Effects of RTK positioning and GCPs

Average offsets in xy and z directions for five surveys per scenario were calculated with all surveys collected on the Phantom 4 platform with either conventional GNSS or RTK positioning (Fig. 3). The baseline scenarios use direct georeferencing only with single survey alignment, resulting in average absolute and relative xy errors with generic GNSS positioning of 175 and 152 cm, respectively. Errors are drastically lower with RTK positioning at 2.0 and 1.0 cm, respectively. Elevation errors also improved when using RTK positioning, but remain relatively high with 67 cm for absolute and 14 cm for relative errors (Fig. 3a). We consider errors up to 2 cm to be below the theoretically limit of our reference data, which means that even without co-alignment, RTK surveys are as accurate as possible for the xy direction. However, z errors were still considerable when using RTK direct georeferencing alone. Errors of direct georeferencing with conventional GNSS were in the range of metres for xy and z, making them unusable for topographic change detection.

Including 5 GCPs per survey greatly improved accuracy when using generic GNSS with average errors of 3.7 cm for xy and 4.7 cm for z directions. With RTK positioning, the absolute elevation error is reduced to 1.3 cm where other errors were already below our detection limit (Fig. 3b). Co-alignment shows modest improvement of absolute accuracies for all scenarios, but relative errors using both RTK and generic GNSS positioning are reduced to below 1 cm for both xy and z (Fig. 3c). When co-alignment was combined with GCPs, the average absolute errors of the general GNSS scenario were 10 cm in xy and 7.0 cm in z. On the other hand, combining co-alignment with GCPs for RTK surveys, shows a reduction of absolute errors to 1.8 and 1.2 cm for xy and z, respectively (Fig. 3d). No differences were apparent in relative errors for both scenarios which were already below the expected detection limit.

### 3.2. Co-alignment of surveys with mixed positioning and GCPs

Fig. 4 shows a grid with results of all co-alignment scenarios with mixed positioning accuracy horizontally and surveys with GCPs digitized vertically. Similar to the results in Fig. 3, relative errors between any of the co-aligned surveys were always below 1 cm in both xy and z directions. Absolute errors were found to depend more strongly on the inclusion of GCPs or RTK positioning, but improve little when digitizing GCPs in multiple surveys or increasing the number of RTK surveys.

Without GCPs, absolute xy errors improved from 127 cm to 1.4 cm when including a single RTK survey in co-alignment. These errors remain below 2 cm when adding a second, or all RTK surveys. Absolute z errors are comparatively high without GCPs and are on average 462, 186, 63 and 53 cm when including 0, 1, 2 and 5 RTK surveys, respectively (Fig. 4a). Digitizing GCPs in a single survey results in both xy and z errors below 10 cm when no RTK surveys are present and to below 2 cm when one or more RTK surveys are included. Adding GCPs to more than one survey, or having more than one RTK survey, does not significantly reduce the absolute errors (students *t*-test on mean survey errors: $\alpha = 0.05$) compared with a single RTK survey with GCPs on 4 lower accuracy missions. This means that when combining multiple surveys, it is sufficient to have a single survey with GCPs and only one survey with RTK photo positioning to minimize positioning errors of the entire project when using co-alignment.

The mixed scenarios confirm the observations at section 3.1 that digitizing GCPs is necessary to significantly reduce absolute xy and z errors for the generic GNSS surveys, while it is necessary for only the z errors for scenarios with at least one RTK survey.

### 3.3. Co-alignment of surveys with different grade sensors and positioning

Co-alignment of images results in comparable improvements when combining survey grade images of RTK positioning with images acquired through a consumer grade UAV with only generic GNSS positioning (Fig. 5). The absolute errors show that co-alignment of Mavic 2 surveys with either 1 or 2 Phantom 4 RTK surveys, is sufficient to reduce

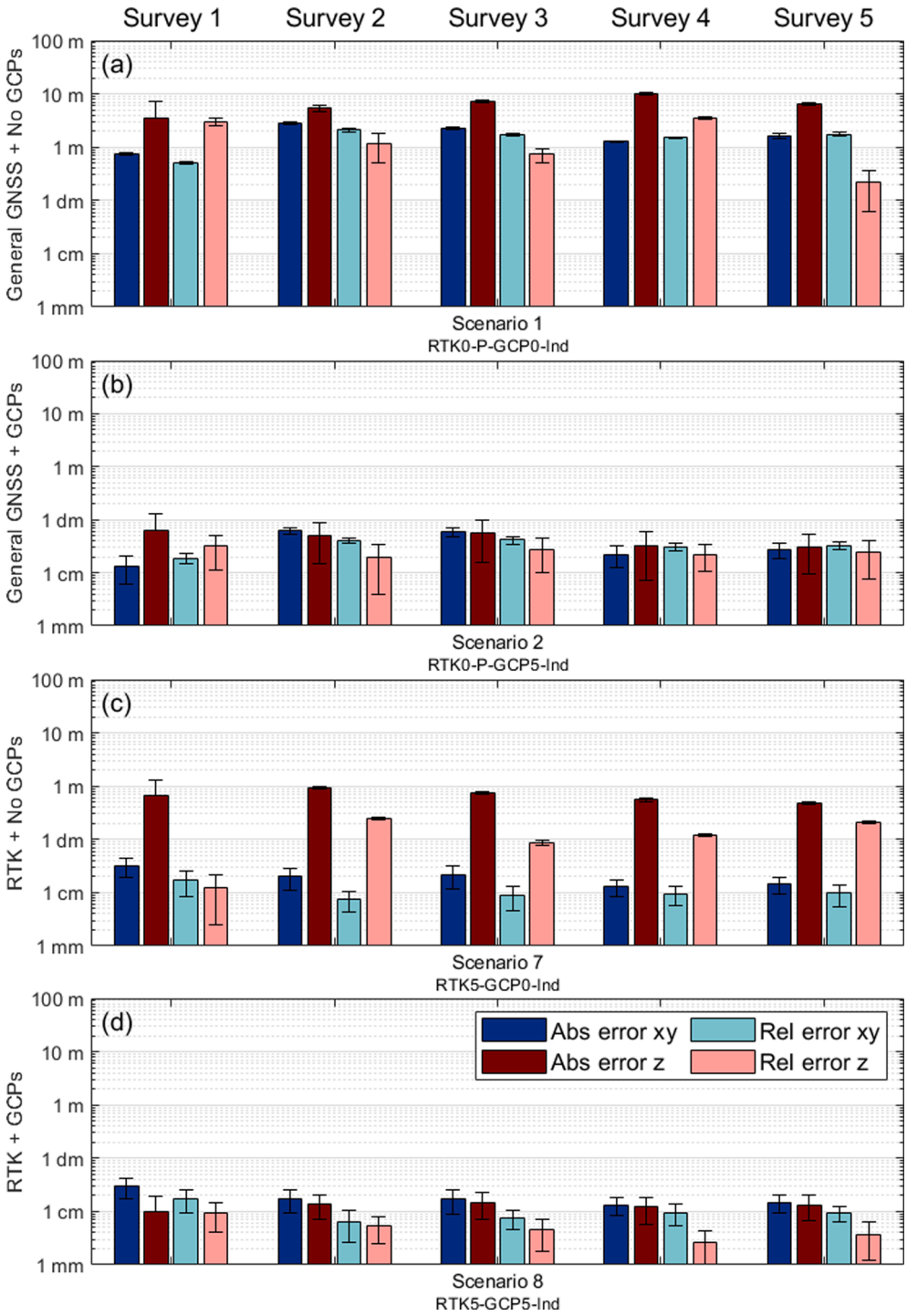


**Fig. 6.** Mean xy and z absolute and relative errors for the (a) full general GNSS without GCPs; (b) full general GNSS with GCPs; (c) full RTK without GCPs; and (d) full RTK with GCPs scenarios divided for each survey on logarithmic scales. Co-alignment was not applied in these scenarios. The scenario numbers and respective ID's below each set refer to Table 1. Whiskers on the bars indicate standard deviations.

the absolute xy error for the Mavic 2 surveys to 3.4 and 1.8 cm, respectively. For the absolute z errors, these values are 20 and 12 cm, respectively, which is even below the absolute z error of 53 cm for the scenario with only Phantom 4 RTK surveys without GCPs.

Digitizing GCPs for all surveys (RTK5-GCP5-CA; RTK2-M-GCP5-CA; RTK1-M-GCP5-CA) results in no significant difference in the xy errors (students *t*-test on mean survey errors: $\alpha = 0.05$). However, adding GCPs shows an improvement of the absolute z errors from 20 to 1.8 cm for co-aligning with 1 RTK survey and from 12 to 1.4 cm for co-aligning with 2 RTK surveys. As was also observed in sections 3.1 and 3.2, Fig. 5 shows that co-alignment results in relative xy and z errors well below 2 cm (between 0.26 and 0.59 cm), meaning optimal relative accuracy is obtained regardless the of amount of RTK surveys as well as whether GCPs are digitized or not.

### 3.4. Variations between surveys

All average errors and their standard deviations of the Phantom 4 surveys that were processed individually, without co-alignment, while varying between RTK settings and whether GCPs are digitized (RTK0-P-GCP0-Ind; RTK0-P-GCP5-Ind; RTK5-GCP0-Ind; RTK5-GCP5-Ind), are

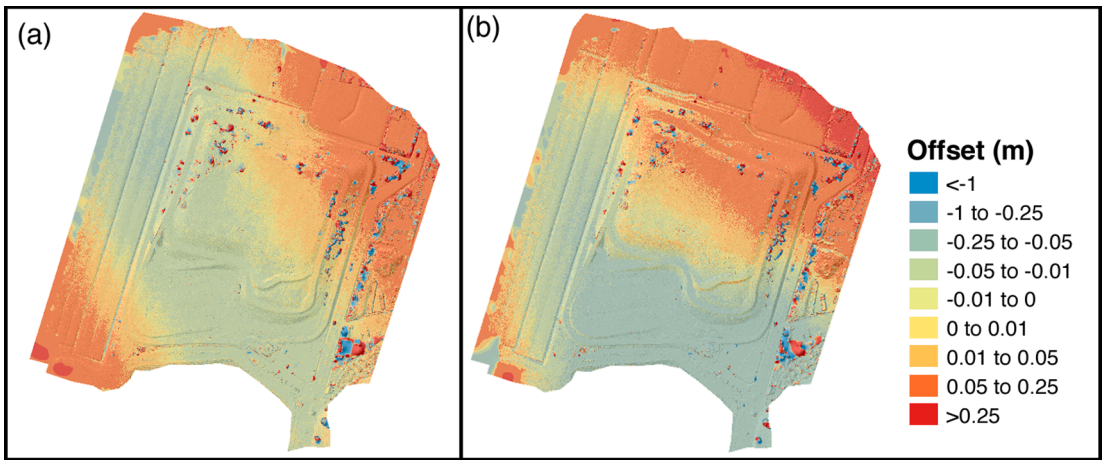


**Fig. 7.** Dome-shaped offsets in the DoDs generated from the fifth survey of (a) general GNSS surveys with GCPs without co-alignment (RTK0-P-GCP5-Ind); and (b) general GNSS surveys with co-alignment with GCPs for 1 survey (RTK0-P-GCP1-CA). The reference DSM is picked from the scenario with the lowest overall errors, which is co-alignment of 2 RTK scenarios with 3 general GNSS scenarios with GCPs digitized for 1 survey (RTK2-P-GCP1-CA). Of this survey, a transparent hillshade is included for both maps. The highest and lowest offsets occur at trees.

given in Fig. 6. As can be observed for the surveys used in this study, we find an inconsistency in especially z accuracy for RTK surveys between different scenarios. All subplots in Fig. 6 show inconsistencies for all errors. These are usually within the same order of magnitude, but can especially differ for relative z errors without GCPs. Fig. 6 also shows that an even more profound inconsistency can be expected for general GNSS surveys than for RTK surveys, due to their lower precision. These differences between surveys can also explain the minor differences in results between co-aligning 1 or 2 RTK surveys with general GNSS Phantom or Mavic surveys (Fig. 5), as well as the surprising results of better performance of co-aligning 2 RTK surveys with 3 general GNSS Phantom surveys over co-aligning 5 RTK surveys with and without GCPs (Fig. 4), while the reverse is true for z errors without GCPs (RTK2-P-GCP0-CA compared to RTK5-GCP0-CA). Although these performance differences are minor in this study, it has not been studied what the full extent of accuracy improvement is by pre-selecting which RTK survey to use for co-alignment. It may therefore be beneficial to quantify errors by first individually processing RTK surveys and then choose the most accurate survey to use for co-alignment when aiming for the last marginal gains in positioning accuracy.

## 4. Discussion

### 4.1. Improvements by RTK settings on direct georeferencing

The results show that DSMs generated by SfM photogrammetry from Phantom 4 surveys with RTK disabled (RTK0-P-GCP0-Ind), result in both absolute as well as relative errors that can be up to several metres, comparable to the findings of previous studies (Turner et al., 2012; Zhang et al., 2019), making these errors too large for the vast majority of change detection studies.

The Phantom 4 surveys with RTK enabled (RTK5-GCP0-Ind), result in significant decreases of all studied errors, where the absolute and relative xy errors decreased below 2 cm, which is the theoretical maximum accuracy. However, absolute and relative z errors of DSMs generated by these surveys are still in the order of several tens of centimetres. These results are comparable to the findings of numerous previous studies on the absolute errors (Gerke & Przybilla, 2016; Benassi et al., 2017; Forlani et al., 2018; Rabah et al., 2018; Tomaštík et al., 2019; Zhang et al., 2019; Przybilla et al., 2020), although these studies show z offsets which are generally two to six times smaller than the absolute z errors found in this study, whereas Gabrlik et al. (2018) find even lower and negligible absolute z errors. This implies that a significant inconsistency related to absolute z accuracy of RTK surveys with direct georeferencing should be considered. This inconsistency can be explained by the differences in accuracy between surveys mentioned in section 3.4 and shows that applying direct georeferencing in UAV-SfM photogrammetry of only RTK surveys may not be sufficient for generating accurate DSMs that can be used for change detection.

### 4.2. Extent of improvements due to GCPs on the UAV-SfM approach without co-alignment

This study further shows that adding GCPs to generate DSMs by SfM photogrammetry from Phantom 4 surveys with RTK disabled (RTK0-P-GCP5-Ind) greatly improves the accuracy, resulting in both absolute as well as relative errors in the order of several centimetres, comparable to findings of previous studies (Turner et al., 2012; Carbonneau & Dietrich, 2017; Stöcker et al., 2017; Zhang et al., 2019). This makes these DSMs applicable for change detection studies, albeit they are still slightly above the theoretically best error margin of 2 cm. Compared to the previous section, this implies that GCPs are necessary for obtaining relatively reliable DSMs generated from general GNSS surveys.

Adding GCPs to the Phantom 4 surveys with RTK enabled (RTK5-GCP5-Ind), results in decreases of all studied errors to below 2 cm. This means that indirect georeferencing is necessary for SfM photogrammetry of RTK surveys to obtain the lowest possible absolute and relative z errors, as opposed to the absolute and relative xy errors, which are already optimized by RTK processing. The effect of GCPs for optimizing absolute z errors of DSMs generated from RTK surveys agrees with the results of previous studies (Fazeli et al., 2016; Gerke & Przybilla, 2016; Benassi et al., 2017; Forlani et al., 2018; Przybilla et al., 2020). Moreover, several studies found that at least one GCP is sufficient to reduce the absolute z error to the extent of the xy errors (Benassi et al., 2017; Forlani et al., 2018; Przybilla et al., 2020). Contrarily to De Haas et al. (2021), this study found no relationship between error and distance to nearest GCP. An explanation for this can be the much smaller study site and relatively close proximity of all VPs to the nearest GCP.

### 4.3. Improvements by co-alignment on the UAV-SfM approach

From the results, it becomes clear that combining direct georeferencing with co-alignment to generate DSMs by SfM photogrammetry, from Phantom 4 surveys with both RTK disabled (RTK0-P-GCP0-CA) as well as RTK enabled (RTK5-GCP0-CA), greatly improves the relative accuracy in both xy and z directions to below 2 cm. Given our ground sampling distance (GSD) of 2.5 cm, this implies that the relative xy and z errors are around 0.2 GSD. This is a great improvement to the 1 GSD for

xy and 2–3 GSD for z found by Aicardi et al. (2016), who applied a co-registration technique by aligning multiple surveys to a reference survey with fixed orientation parameters, as opposed to the bundle adjustment of co-alignment used in this study. Despite a slight improvement of both absolute xy and z accuracy, the xy and z errors remain in the same order as without co-alignment. This means that only co-alignment of general GNSS surveys is insufficient to properly minimize both absolute xy and z errors, while only co-alignment of RTK surveys is insufficient to properly minimize the absolute z errors.

Przybilla et al. (2020) found distinctive dome-shaped absolute error distributions for DSMs generated with GCPs without RTK settings without co-alignment. In this study, DoDs were created for the fifth survey of all scenarios with the reference scenario with the overall lowest error (RTK2-P-GCP1-CA; RTK2-P-GCP2-CA; RTK2-P-GCP5-CA). As there is statistically no difference between those three scenarios, the one with the lowest computational time of digitizing GCPs for only one survey was chosen (RTK2-P-GCP1-CA). The DoDs show that this dome-shaped feature is only recognizable for the scenarios of indirectly georeferenced general GNSS surveys (RTK0-P-GCP5-Ind; RTK0-P-GCP1-CA; RTK0-P-GCP2-CA; RTK0-P-GCP5-CA; Fig. 7), as was the case for the results of Przybilla et al. (2020). This means that this feature should be considered when geoprocessing general GNSS surveys with GCPs. Contrarily to considerations mentioned by Cook & Dietze (2019) and De Haas et al. (2021), distinctive dome shapes were not identified in other scenarios where co-alignment was applied. This implies that RTK settings in at least one survey are sufficient to prevent doming structures in the absolute errors. This further means that the higher absolute errors in xy and z direction for co-aligning general GNSS surveys and in z direction for co-aligning RTK surveys, become systematic. This is confirmed by the low average standard deviations of the absolute errors of the co-alignment scenarios with at least 1 RTK survey (Figs. 4 and 5), which are below 2 cm for all absolute xy errors, below 2 cm for the absolute z errors with GCPs and below 4 cm for the absolute errors in z direction without GCPs. The only exception here is RTK1-P-GCP0-CA, where 1 RTK survey is co-aligned with 4 general GNSS surveys without GCPs, where the standard deviation of the absolute z errors is 9.6 cm (Fig. 5). This underlines the effectiveness of combining GCPs with co-alignment, which is also discussed in previous studies for both RTK surveys (Hendrickx et al., 2020), as well as general GNSS surveys (De Haas et al., 2021; Parente et al., 2021). Nevertheless, as is pointed out by De Haas et al. (2021) and Saponaro et al. (2021) , co-alignment has the ability to force surveys of poor quality to a common geometry which is more robust and applicable for change detection, indicating that a higher systematic error is not a problem for change detection as long as there is a low relative error. This is confirmed by Li et al. (2017), who state that a high-resolution absolute positioning of survey imagery is not necessary for change detection studies, as co-alignment forces a local coordinate system with low relative errors.

Cook & Dietze (2019) found almost identical results for DoDs created through the co-alignment workflow compared to GCPs, while the results of De Haas et al. (2021) showed even better results for the relative errors of DSMs created through co-alignment without GCPs than through individual processing of surveys with GCPs (no co-alignment). The latter is also the case for our study for both RTK surveys as well as general GNSS surveys (RTK0-P-GCP5-Ind; RTK0-P-GCP0-CA; RTK5-GCP5-Ind; RTK5-GCP0-CA; Fig. 3), where the relative xy errors increase from 0.6 to 1.0 cm for RTK and from 0.6 to 3.3 cm for general GNSS for the co-alignment workflow to the GCP workflow, respectively. For the relative z errors, there is an increase from 0.3 to 0.5 cm for RTK and from 0.3 to 2.5 cm for general GNSS, respectively. The robustness of the co-alignment approach to greatly reduce relative errors is confirmed by the study of Blanch et al. (2021), who showed absolute and relative errors of below 2 cm for a fully automated workflow of change detection using co-alignment without GCPs for a cliff. Nevertheless, it should be considered that a prerequisite for co-alignment is the presence of sufficient stable areas over time (Feurer & Vinatier, 2018; Cook & Dietze, 2019; Li et al., 2020).

With respect to combining GCPs and co-alignment for creating DSMs and DoDs with both low relative accuracy and low absolute accuracy, a statistically substantiated finding in this study is that when combining co-alignment with GCPs, it is sufficient to digitize the GCPs for only one survey, saving a great deal of time in the data processing step. Furthermore, combining co-alignment and GCPs can result in reliable DSMs, where the absolute xy, relative xy, absolute z and relative z errors remain below 2 cm. These low overall errors in several scenarios confirm the findings by Feurer & Vinatier (2018), who concluded that co-alignment is a useful tool for determining change detection on smaller scales than previously possible. They moreover found that only a limited number of GCPs is sufficient for creating reliable DSMs and DoDs, also as a result of the common geometry forced through co-alignment. Furthermore, as is pointed out by Parente et al. (2021), there is need for GCPs if a highly accurate photogrammetric geometric dataset is unavailable. This study shows that when using co-alignment, this geometric dataset is essentially created when the GCPs are digitized for 1 RTK survey. This suggests that the accuracy of DSMs of old surveys, conducted with lower-quality sensors and UAVs, can be upgraded by co-alignment with 1 RTK survey where GCPs are digitized towards an RTK accuracy. This may open up a path towards high-accuracy change detection studies of times before RTK-UAVs were even available.

Furthermore, the scenarios with generic GNSS Mavic surveys (RTK1-M-GCP0-CA; RTK1-M-GCP5-CA; RTK2-M-GCP0-CA; RTK2-M-GCP5-CA) show that co-alignment of an older, lower-quality sensor such as the Mavic 2 Pro with RTK surveys of the Phantom 4, results in decent DSMs, where the surveys of the Mavic are forced onto the accurate geometry of the Phantom 4 RTK. This is in line with the findings of Hendrickx et al. (2020), who co-aligned a Phantom 4 survey with 2 Hexacopter DJI F550 surveys, resulting in the removal of the systematic error of the latter surveys. Parente et al. (2021) additionally showed that UAV imagery can effectively be co-aligned with terrestrial imagery, under different weather conditions, resulting in very small relative errors. This is also in line with our study, where the different weather conditions of sunny and partially clouded provided no problems for the co-alignment processing step.

Because the conditions in this study were deliberately idealized, lacking any mentionable change between the surveys, apart from the weather conditions, the results in this study may differ from situations with much change. Nevertheless, co-alignment proves to be a robust method for studying change in areas with sufficient stable areas to enable image co-alignment, as has been shown by the results of previous studies with substantial change (Cook & Dietze, 2019; De Haas et al., 2021). This implies that the results in this study, despite the idealized situations, give relationships that are representative for other situations of different spatial and temporal scales. Nevertheless, as is pointed out by Feurer & Vinatier (2018), there should still be sufficient stable multi-temporal tie points in order to make co-alignment succeed.

Moreover, our study area is relatively small, allowing for relatively fast computation times. Yet the study of De Haas et al. (2021) shows that co-aligning up to 10 sets of an area of with over 1000 images along a stretch of about 1 km is still feasible. It must be noted here that such computing may be very time-consuming on a general desktop and is therefore ideally conducted through a computer cluster.

In short, in this study average relative and absolute errors in both xy and z direction below 2 cm were obtained for several scenarios. Our data suggests that for creating high-accuracy DoDs, it is sufficient to only apply co-alignment to reduce the relative errors to a minimum, regardless of whether RTK is enabled or not. For reducing the absolute xy errors, we advise to apply co-alignment with at least 1 RTK survey, which could be a solution for challenging, inaccessible terrains where GCPs are not feasible. In contrast to previous studies, the RTK surveys of this study are, however, insufficient to properly improve absolute and relative z errors to the accuracy of 2 cm. Nevertheless, RTK surveys work well in preventing a doming distribution of absolute errors, which is observed for general GNSS surveys. In order to minimize the z errors, we

advise digitizing GCPs for 1 RTK survey, as there is no improvement in errors when GCPs are digitized for more surveys. When co-aligning general GNSS surveys with a lower-quality sensor, such as the Mavic 2 Pro, the data in this study suggests that it is best to combine GCPs with co-alignment with at least 2 RTK surveys, or with 1 RTK survey which is pre-selected to be the most accurate.

## 5. Conclusions

We present a thorough analysis of 24 workflows for creating DSMs through UAV-SfM photogrammetry, exploring the potential for minimizing both absolute and relative errors of mixed scenarios where co-alignment is combined with mixed survey grades, RTK surveys, and ground control. The scenarios provide guidance to find the best possible workflow for change detection as well as an indication of expected accuracies from a controlled case to support realistic expectations and selection of further analysis strategies, especially when high quality positioning or ground control is unavailable for part of the surveys.

We show that the general approach of UAV-SfM for general GNSS UAV surveys without GCPs or co-alignment produces DSMs with both absolute and relative errors that are too large for detailed change detection. Applying UAV-SfM to RTK surveys partially overcomes this problem by greatly improving both absolute and relative xy errors to below 2 cm, but z errors may remain greater than 10 cm and thus insufficient. For all scenarios, co-alignment greatly improves relative errors to below 2 cm but absolute accuracy is only improved slightly. Using GCPs does successfully counter the problem of high z errors for RTK surveys to below 2 cm, as well as improve both xy and z errors of general GNSS surveys to an acceptable accuracy of $\sim$ 4 cm.

Co-alignment with at least 1 RTK survey improves the accuracy of the DSM generated by the general GNSS survey up to the accuracy of an RTK survey and prevents a doming distribution of absolute z errors, which is common in general GNSS surveys. The benefits of co-alignment also hold when surveys were conducted with a different sensor. When using co-alignment, we found no difference in accuracy between scenarios where GCPs were digitized for either 1, 2 or all surveys.

Both absolute and relative errors of several tested workflows are below 2 cm, which is the theoretical maximum accuracy given pixel size and reference point precision. Our results open up a path towards high-accuracy change detection studies including images acquired before RTK-UAVs were available or with GCPs present in only a single survey. To obtain maximum accuracy in minimum time, we show that future UAV-SfM photogrammetry studies that focus on change detection ideally (i) apply co-alignment with at least 1 RTK survey, (ii) and digitize GCPs for only 1 survey, instead of digitizing GCPs for each survey.

## CRediT authorship contribution statement

**E.W. Nota:** Data curation, Formal analysis, Funding acquisition, Investigation, Methodology, Software, Validation, Visualization, Writing – original draft, Writing – review & editing. **W. Nijland:** Conceptualization, Investigation, Methodology, Software, Writing – review & editing. **T. de Haas:** Conceptualization, Data curation, Funding acquisition, Investigation, Methodology, Writing – review & editing.

## Declaration of Competing Interest

The authors declare that they have no known competing financial interests or personal relationships that could have appeared to influence the work reported in this paper.

## Acknowledgements

This work was funded by the Netherlands Organization for Scientific Research (NWO) (Grant No. 016.Veni.192.001 to TdH). Additional funding came from a Bright Minds Assistantship from the Faculty of Geosciences of Utrecht University, The Netherlands.

## Appendix

Table A1.

**Table A1**
Average results of the absolute and relative xy and z errors as well as their standard deviations in cm.

| Scenario | Nr. RTK surveys | Nr. No-RTK surveys | Co-alignment | GCPs | Nr. Surveys with GCPs | No-RTK surveys sensor | Av. abs. xy error (cm) | Av. abs. z error (cm) | Av. rel. xy error (cm) | Av. rel z error (cm) | Av. stdv. abs. xy error (cm) | Av. stdv. abs. z error (cm) | Av. stdv. rel. xy error (cm) | Av. stdv. rel. xy error (cm) |
|---|---|---|---|---|---|---|---|---|---|---|---|---|---|---|
| 1 | 0 | 5 | No | No | 0 | Phantom | 174.7 | 653.2 | 152.0 | 170.6 | 11.13 | 52.35 | 10.69 | 32.94 |
| 2 | 0 | 5 | No | Yes | 5 | Phantom | 3.680 | 4.736 | 3.323 | 2.487 | 0.918 | 3.194 | 0.508 | 1.610 |
| 3 | 0 | 5 | Yes | No | 0 | Phantom | 126.6 | 462.4 | 0.596 | 0.257 | 6.615 | 31.32 | 0.316 | 0.172 |
| 4 | 0 | 5 | Yes | Yes | 5 | Phantom | 9.965 | 7.000 | 0.612 | 0.262 | 1.057 | 4.377 | 0.292 | 0.177 |
| 5 | 0 | 5 | Yes | Yes | 1 | Phantom | 9.854 | 7.255 | 0.543 | 0.277 | 1.078 | 4.525 | 0.284 | 0.188 |
| 6 | 0 | 5 | Yes | Yes | 2 | Phantom | 9.737 | 7.088 | 0.568 | 0.271 | 1.064 | 4.457 | 0.287 | 0.179 |
| 7 | 5 | 0 | No | No | 0 | | 2.014 | 67.46 | 1.048 | 13.54 | 0.806 | 3.915 | 0.477 | 0.994 |
| 8 | 5 | 0 | No | Yes | 5 | | 1.852 | 1.279 | 1.005 | 0.513 | 0.783 | 0.686 | 0.432 | 0.301 |
| 9 | 5 | 0 | Yes | No | 0 | | 1.845 | 53.17 | 0.569 | 0.265 | 0.728 | 3.163 | 0.299 | 0.182 |
| 10 | 5 | 0 | Yes | Yes | 5 | | 1.763 | 1.209 | 0.582 | 0.279 | 0.710 | 0.865 | 0.363 | 0.205 |
| 11 | 5 | 0 | Yes | Yes | 1 | | 1.827 | 1.145 | 0.573 | 0.281 | 0.672 | 0.828 | 0.311 | 0.203 |
| 12 | 5 | 0 | Yes | Yes | 2 | | 1.714 | 1.052 | 0.561 | 0.277 | 0.637 | 0.799 | 0.307 | 0.193 |
| 13 | 1 | 4 | Yes | No | 0 | Phantom | 1.360 | 186.1 | 0.466 | 0.355 | 0.620 | 9.606 | 0.260 | 0.212 |
| 14 | 1 | 4 | Yes | Yes | 5 | Phantom | 1.305 | 1.018 | 0.449 | 0.401 | 0.541 | 1.029 | 0.236 | 0.252 |
| 15 | 1 | 4 | Yes | Yes | 1 | Phantom | 1.409 | 1.012 | 0.526 | 0.378 | 0.561 | 1.124 | 0.256 | 0.244 |
| 16 | 1 | 4 | Yes | Yes | 2 | Phantom | 1.424 | 1.044 | 0.496 | 0.411 | 0.562 | 1.076 | 0.227 | 0.265 |
| 17 | 2 | 3 | Yes | No | 0 | Phantom | 1.358 | 62.73 | 0.517 | 0.270 | 0.568 | 3.727 | 0.275 | 0.176 |
| 18 | 2 | 3 | Yes | Yes | 5 | Phantom | 1.374 | 0.938 | 0.544 | 0.310 | 0.584 | 0.668 | 0.252 | 0.224 |
| 19 | 2 | 3 | Yes | Yes | 1 | Phantom | 1.348 | 0.982 | 0.518 | 0.296 | 0.549 | 0.690 | 0.257 | 0.236 |
| 20 | 2 | 3 | Yes | Yes | 2 | Phantom | 1.366 | 0.979 | 0.481 | 0.284 | 0.598 | 0.654 | 0.275 | 0.233 |
| 21 | 2 | 3 | Yes | No | 0 | MAVIC | 1.853 | 12.47 | 0.825 | 0.582 | 1.538 | 1.874 | 0.932 | 0.469 |
| 22 | 2 | 3 | Yes | Yes | 5 | MAVIC | 1.807 | 1.383 | 0.833 | 0.597 | 1.376 | 0.908 | 0.776 | 0.446 |
| 23 | 1 | 4 | Yes | No | 0 | MAVIC | 3.385 | 19.79 | 0.713 | 0.548 | 1.922 | 2.604 | 0.613 | 0.544 |
| 24 | 1 | 4 | Yes | Yes | 5 | MAVIC | 3.317 | 1.804 | 0.698 | 0.585 | 1.809 | 1.426 | 0.608 | 0.804 |

## References


Aicardi, I., Nex, F., Gerke, M., Lingua, A.M., 2016. An image-based approach for the co-registration of multi-temporal UAV image datasets. Remote sensing 8 (9), 779.

Anderson, K., Westoby, M.J., James, M.R., 2019. Low-budget topographic surveying comes of age: Structure from motion photogrammetry in geography and the geosciences. Progress in Physical Geography: Earth and Environment 43 (2), 163–173.

Bakker, M., Lane, S.N., 2017. Archival photogrammetric analysis of river–floodplain systems using Structure from Motion (SfM) methods. Earth Surface Processes and Landforms 42 (8), 1274–1286.

Benassi, F., Dall'Asta, E., Diotri, F., Forlani, G., Morra di Cella, U., Roncella, R., Santise, M., 2017. Testing accuracy and repeatability of UAV blocks oriented with GNSS-supported aerial triangulation. Remote Sensing 9 (2), 172.

Blanch, X., Eltner, A., Guinau, M., Abellan, A., 2021. Multi-Epoch and Multi-Imagery (MEMI) Photogrammetric Workflow for Enhanced Change Detection Using Time-Lapse Cameras. Remote Sensing 13 (8), 1460.

Cabo, C., Sanz-Ablanedo, E., Roca-Pardinas, J., Ordonez, C., 2021. Influence of the number and spatial distribution of ground control points in the accuracy of uav-sfm dems: an approach based on generalized additive models. IEEE Transactions on Geoscience and Remote Sensing 59 (12), 10618–10627.

Carbonneau, P.E., Dietrich, J.T., 2017. Cost-effective non-metric photogrammetry from consumer-grade sUAS: implications for direct georeferencing of structure from motion photogrammetry. Earth Surface Processes and Landforms 42 (3), 473–486.

Cook, K.L., 2017. An evaluation of the effectiveness of low-cost UAVs and structure from motion for geomorphic change detection. Geomorphology 278, 195–208.

Cook, K.L., Dietze, M., 2019. A simple workflow for robust low-cost UAV-derived change detection without ground control points. Earth Surface Dynamics 7 (4), 1009–1017.

De Haas, T., Nijland, W., De Jong, S.M., McArdell, B.W., 2020. How memory effects, check dams, and channel geometry control erosion and deposition by debris flows. Scientific reports 10 (1), 1–8.

De Haas, T., Nijland, W., McArdell, B.W., Kalthof, M.W., 2021. Case Report: Optimization of Topographic Change Detection With UAV Structure-From-Motion Photogrammetry Through Survey Co-Alignment. Frontiers in Remote Sensing 2, 5.

Dietze, M., Cook, K. L., Illien, L., Rach, O., Puffpaff, S., Stodian, I., & Hovius, N. (2020). Impact of nested moisture cycles on coastal chalk cliff failure revealed by multiseasonal seismic and topographic surveys. *Journal of Geophysical Research: Earth Surface*, *125*(8), e2019JF005487.

Dille, A., Kervyn, F., Handwerger, A.L., d'Oreye, N., Derauw, D., Mugaruka Bibentyo, T., Samsonov, S., Malet, J.-P., Kervyn, M., Dewitte, O., 2021. When image correlation is needed: Unravelling the complex dynamics of a slow-moving landslide in the tropics with dense radar and optical time series. Remote Sensing of Environment 258, 112402.

Fazeli, H., Samadzadegan, F., Dadrasjavan, F., 2016. Evaluating the potential of RTK-UAV for automatic point cloud generation in 3D rapid mapping. The International Archives of Photogrammetry, Remote Sensing and Spatial Information Sciences 41, 221.

Feurer, D., Vinatier, F., 2018. Joining multi-epoch archival aerial images in a single SfM block allows 3-D change detection with almost exclusively image information. ISPRS journal of photogrammetry and remote sensing 146, 495–506.

Fojtik, A. C. (2020). *Short-term response of a mountain stream to a sediment pulse and a major flood* (Doctoral dissertation).

Fonstad, M.A., Dietrich, J.T., Courville, B.C., Jensen, J.L., Carbonneau, P.E., 2013. Topographic structure from motion: a new development in photogrammetric measurement. Earth surface processes and Landforms 38 (4), 421–430.

Forlani, G., Dall'Asta, E., Diotri, F., Cella, U.M.d., Roncella, R., Santise, M., 2018. Quality assessment of DSMs produced from UAV flights georeferenced with on-board RTK positioning. Remote Sensing 10 (2), 311.

Gabrlik, P., Cour-Harbo, A.L., Kalvodova, P., Zalud, L., Janata, P., 2018. Calibration and accuracy assessment in a direct georeferencing system for UAS photogrammetry. International journal of remote sensing 39 (15–16), 4931–4959.

Gerke, M., Przybilla, H.-J., 2016. Accuracy analysis of photogrammetric UAV image blocks: Influence of onboard RTK-GNSS and cross flight patterns. *Photogrammetrie, Fernerkundung*. Geoinformation (PFG) 2016 (1), 17–30.

Hendrickx, H., De Sloover, L., Stal, C., Delaloye, R., Nyssen, J., Frankl, A., 2020. Talus slope geomorphology investigated at multiple time scales from high-resolution topographic surveys and historical aerial photographs (Sanetsch Pass, Switzerland). Earth Surface Processes and Landforms 45 (14), 3653–3669.

James, M.R., Robson, S., Smith, M.W., 2017. 3-D uncertainty-based topographic change detection with structure-from-motion photogrammetry: Precision maps for ground control and directly georeferenced surveys. Earth Surface Processes and Landforms 42 (12), 1769–1788.

Jester, W., Klik, A., 2005. Soil surface roughness measurement—methods, applicability, and surface representation. Catena 64 (2–3), 174–192.

Li, W., Sun, K., Li, D., Bai, T., Sui, H., 2017. A new approach to performing bundle adjustment for time series UAV images 3D building change detection. Remote sensing 9 (6), 625.

Li, T., Zhang, B., Xiao, W., Cheng, X., Li, Z., Zhao, J., 2020. UAV-Based Photogrammetry and LiDAR for the Characterization of Ice Morphology Evolution. IEEE Journal of Selected Topics in Applied Earth Observations and Remote Sensing 13, 4188–4199.

Nebiker, S., Annen, A., Scherrer, M., Oesch, D., 2008. A light-weight multispectral sensor for micro UAV—Opportunities for very high resolution airborne remote sensing. Int. Arch. Photogramm. Remote Sens. Spat. Inf. Sci 37 (B1), 1193–1200.

Rabah, M., Basiouny, M., Ghanem, E., Elhadary, A., 2018. Using RTK and VRS in direct geo-referencing of the UAV imagery. NRIAG Journal of Astronomy and Geophysics 7 (2), 220–226.

Parente, L., Chandler, J.H., Dixon, N., 2021. Automated Registration of SfM-MVS Multitemporal Datasets Using Terrestrial and Oblique Aerial Images. The Photogrammetric Record 36 (173), 12–35.

Pfeifer, N., Glira, P., Briese, C., 2012. Direct georeferencing with on board navigation components of light weight UAV platforms. International Archives of the Photogrammetry, Remote Sensing and Spatial Information Sciences 39 (B7), 487–492.

Przybilla, H.J., Bäumker, M., Luhmann, T., Hastedt, H., Eilers, M., 2020. Interaction between direct georeferencing, control point configuration and camera self-calibration for rtk-based uav photogrammetry. The International Archives of Photogrammetry, Remote Sensing and Spatial Information Sciences 43, 485–492.

Sanz-Ablanedo, E., Chandler, J.H., Rodríguez-Pérez, J.R., Ordóñez, C., 2018. Accuracy of unmanned aerial vehicle (UAV) and SfM photogrammetry survey as a function of the number and location of ground control points used. Remote Sensing 10 (10), 1606.

Saponaro, M., Capolupo, A., Caporusso, G., Tarantino, E., 2021. Influence of Co-Alignment Procedures on the Co-Registration Accuracy of Multi-Epoch SFM Points Clouds. The International Archives of Photogrammetry, Remote Sensing and Spatial Information Sciences 43, 231–238.

Smith, M.J., Asal, F.F.F., Priestnall, G., 2004. The use of photogrammetry and lidar for landscape roughness estimation in hydrodynamic studies. ISPRS, XXXB, part B 3, 714–719.

Snavely, K.N., 2008. Scene reconstruction and visualization from internet photo collections. University of Washington.

Stöcker, C., Nex, F., Koeva, M., Gerke, M., 2017. Quality assessment of combined IMU/GNSS data for direct georeferencing in the context of UAV-based mapping. The International Archives of Photogrammetry, Remote Sensing and Spatial Information Sciences 42, 355.

Stempfhuber, W., Buchholz, M., 2011. A precise, low-cost RTK GNSS system for UAV applications. Proc. of Unmanned Aerial Vehicle in Geomatics, ISPRS.

Takasu, T., Yasuda, A., 2009. Development of the low-cost RTK-GPS receiver with an open source program package RTKLIB Vol. 1.

Tomaštík, J., Mokroš, M., Surový, P., Grznárová, A., Merganič, J., 2019. UAV RTK/PPK method—an optimal solution for mapping inaccessible forested areas? Remote sensing 11 (6), 721.

Turner, D., Lucieer, A., Watson, C., 2012. An automated technique for generating georectified mosaics from ultra-high resolution unmanned aerial vehicle (UAV) imagery, based on structure from motion (SfM) point clouds. Remote sensing 4 (5), 1392–1410.

Villanueva, J.K.S., Blanco, A.C., 2019. Optimization of ground control point (GCP) configuration for unmanned aerial vehicle (UAV) survey using structure from motion (SFM). *International Archives of the Photogrammetry, Remote Sensing and Spatial*. Information Sciences XLII-4/W12, 167–174.

Watson, C.S., Kargel, J.S., Shugar, D.H., Haritashya, U.K., Schiassi, E., Furfaro, R., 2020. Mass loss from calving in Himalayan proglacial lakes. Frontiers in Earth Science 7, 342.

Westoby, M.J., Brasington, J., Glasser, N.F., Hambrey, M.J., Reynolds, J.M., 2012. 'Structure-from-Motion'photogrammetry: A low-cost, effective tool for geoscience applications. Geomorphology 179, 300–314.

Wheaton, J.M., Brasington, J., Darby, S.E., Sear, D.A., 2010. Accounting for uncertainty in DEMs from repeat topographic surveys: improved sediment budgets. Earth surface processes and landforms: the journal of the British Geomorphological Research Group 35 (2), 136–156.

Zhang, H., Aldana-Jague, E., Clapuyt, F., Wilken, F., Vanacker, V., Van Oost, K., 2019. Evaluating the Potential of PPK Direct Georeferencing for UAV-SfM Photogrammetry and Precise Topographic Mapping. Earth Surf. Dyn. Discuss 1–34.